AGTR1 potentiates the chemotherapeutic efficacy of cisplatin in esophageal carcinoma through elevation of intracellular Ca^{2+} and induction of apoptosis

KANG LIU[1], JUN BIE[2], RUOLAN ZHANG[1], RONG XIONG[1], LIHONG PENG[1], YI LUO[1], SIYUN YANG[1], GANG FENG[1] and GUIQIN SONG[1,3]

[1]Institute of Tissue Engineering and Stem Cells, Nanchong Central Hospital, The Second Clinical Medical College, North Sichuan Medical College, Nanchong, Sichuan 637000, P.R. China; [2]Department of Oncology, Nanchong Central Hospital, The Second Clinical Medical College, North Sichuan Medical College, Nanchong, Sichuan 637000, P.R. China; [3]School of Basic Medicine and Forensic Sciences, North Sichuan Medical College, Nanchong, Sichuan 637100, P.R. China

Received January 4, 2024; Accepted October 25, 2024

DOI: 10.3892/ijo.2025.5738

Abstract. Cisplatin is one of the principal chemotherapeutic agents used for esophageal cancer (EC) treatment; however, EC mortality remains high. It is therefore imperative to find new therapeutic targets and approaches to potentiate the chemotherapeutic efficacy of cisplatin. Angiotensin II receptor type 1 (AGTR1) is a potential therapeutic target in multiple cancer types. In the present study, RNA-sequencing analysis of EC and normal esophageal tissues was performed and AGTR1 was identified as a differentially expressed gene that is markedly downregulated in recurrent and metastasized EC. AGTR1 upregulation in the esophageal squamous cell carcinoma cell lines, KYSE-150 and EC109, promoted their chemosensitivity to cisplatin both *in vitro* and *in vivo*. Additionally, AGTR1 suppressed the metastasis-relevant traits of EC cells, as evidenced by the reduced migration, invasion and wound healing of EC cells with higher AGTR1 expression levels. Moreover, AGTR1 overexpression in EC cells upregulated intracellular Ca^{2+} levels, reduced ATP levels and mitochondrial membrane potentials, which was accompanied by enhanced mitochondrial pathway apoptosis. Notably, either AGTR1 overexpression or treatments with the calcium channel blocker, fendiline, caused Ca^{2+} influx and promoted mitochondria-dependent apoptosis in KYSE-150 cells *in vitro*. These effects were augmented when both AGTR1 overexpression and fendiline stimulation were imposed in the absence or presence of cisplatin treatments. Furthermore, fendiline administration enhanced the chemosensitivity of cisplatin in an EC xenograft mouse model. Collectively, these findings offer an alternative treatment option and provide mechanistic insights into using fendiline to potentiate the chemotherapy efficacy of cisplatin in treating EC.

Correspondence to: Professor Gang Feng, Institute of Tissue Engineering and Stem Cells, Nanchong Central Hospital, The Second Clinical Medical College, North Sichuan Medical College, 97 People's South Road, Nanchong, Sichuan 637000, P.R. China
E-mail: fenggang@nsmc.edu.cn

Professor Guiqin Song, School of Basic Medicine and Forensic Sciences, North Sichuan Medical College, 55 Dongshun Road, Nanchong, Sichuan 637100, P.R. China
E-mail: songguiqin@nsmc.edu.cn

Key words: esophageal carcinoma, cisplatin, chemosensitivity, AGTR1, Ca^{2+} influx-induced apoptosis, fendiline

Introduction

As one of the most common malignant neoplasms in the digestive tract, esophageal cancer (EC) remains an integral cause of cancer-related death (1). Although the incidence of EC varies considerably with location, the number of global new cases in 2020 was ~604,100, and the mortality caused by EC ranked tenth in terms of malignant tumors (2). EC can be separated by histological type into squamous cell carcinoma, adenocarcinoma, small cell carcinoma and carcinosarcoma. Esophageal squamous cell carcinoma (ESCC) is the predominant histological type worldwide, and accounts for ~90% of all EC cases (3). The management of EC is complex and highly variable between countries and medical centers. Clinically, chemotherapy has been one of the major therapeutic approaches in the trimodal therapy of EC (4). Multimodal therapy refers to neoadjuvant chemoradiotherapy or perioperative chemotherapy combined with esophagectomy, which has been increasingly used worldwide due to its greater survival advantage compared with surgery alone (5). Additionally, despite multimodal treatment, most patients with EC and locally advanced disease will eventually develop metastatic disease, and most patients will receive palliative chemotherapy at some point (6). However, although some progress has been made in multidisciplinary management in recent years, the treatment of EC is still a serious challenge, partly because numerous patients are insensitive or adaptively resistant to chemotherapy drugs (7). Therefore, it is imperative to further elucidate the mechanisms of drug resistance in

EC and develop chemosensitizers and combined therapies to decrease EC mortality.

Cisplatin is one of the principal chemotherapeutic agents used for the first-line treatment of a number of malignancies, including EC (8). In addition, combination therapies with cisplatin and other therapeutics such as 5-fluorouracil remain the most frequently used chemotherapy for ESCC (9). The main anticancer mechanism of cisplatin is that it interacts with purine bases in DNA to form DNA-protein and DNA-DNA inter-strand and intra-strand crosslinks, thereby inhibiting the proliferation and apoptosis of tumor cells (10). It has been proposed that one aspect of the molecular mechanism of cisplatin is the induction of intracellular calcium efflux and subsequent triggering of apoptosis (11). Intracellular calcium ions (Ca^{2+}), as a second messenger, regulate gene transcription, and cell migration, proliferation and death. Evidence has shown that the Ca^{2+} homeostasis in cancer cells is altered, which is related to tumor initiation, angiogenesis, progression and metastasis (11). It has been proposed that reduced calcium influx in cancer cells prevents calcium overload in response to proapoptotic stimuli, thereby impairing the effectiveness of mitochondrial and cytoplasmic apoptotic pathways (12). Moreover, cisplatin-induced cell death is reported to be dependent on calcium/calpain, store-operated calcium entry and calcium efflux in ovarian (13), non-small cell lung (14) and cervical (15) cancer. Thus, it appears that approaches which enhance calcium efflux may contribute to the apoptotic death of cancer cells. However, to the best of our knowledge, how the intracellular calcium stock contributes to the cisplatin-mediated death of EC cells, and whether excessive intracellular calcium can sensitize EC cells to cisplatin remains unexplored so far.

Angiotensin II receptor type 1, also termed the AT1 receptor (AGTR1), is the most characterized angiotensin receptor (16) and is an important effector controlling blood pressure and volume in the cardiovascular system (16). An entire class of AGTR1 receptor blockers are already clinically available (17). AGTR1 has been previously linked to cancer and is considered a therapeutic target in estrogen receptor (ER)-positive and Erb-B2 receptor tyrosine kinase 2-negative breast cancer, as it is upregulated in this cancer type and promotes lymph node metastasis (18-20). In addition, AGTR1 blockade has shown therapeutic effects in ovarian cancer (21). However, repression of AGTR1 contributes to the multi-chemoresistance of osteosarcoma (22), and high AGTR1 expression was reported to induce apoptosis in β-cell and islet (23,24), intestinal epithelial (25) and cardiac (26) cells. These results suggest that AGTR1 may function as an oncogenic factor in some cancer types while its upregulation can induce apoptosis in multiple cell types. However, to the best of our knowledge, utilization of the pro-apoptotic property of AGTR1 to eliminate malignancies and the potential mechanisms in EC have not yet been explored.

In the present study, the gene expression profiles of EC and normal esophageal tissues were compared. To analyze the association between AGTR1 expression and chemosensitivity of EC tumors to cisplatin, KYSE-150 cells with a low AGTR1 expression level and EC109 cells with a high AGTR1 expression level were used. In addition, the effect of combined treatment with cisplatin and the nonselective calcium channel blocker fendiline was evaluated using an EC xenograft model. In clinical practice, the results of the present study may provide an alternative treatment option with an improved prognosis for patients with EC.

Materials and methods

Patients and clinical sample preparation. The tumor tissue specimens were collected from patients with EC who underwent surgical resection between December 2019 and June 2021 in the Department of Thoracic Surgery of Nanchong Central Hospital (Nanchong, China). The age of patients ranged between 48 and 75 years (mean age, 63.67 years; median age, 65 years), with 50% male and 50% female patients. The inclusion criteria were: Age ≥18 years; the medical records were complete; and the patient was diagnosed with esophageal cancer. The exclusion criteria were: Combined with other malignant tumors; the telephone number and other contact information were missing; and those with incomplete follow-up information. These patients received a standardized treatment protocol consisting of neoadjuvant chemotherapy with cisplatin followed by appropriate surgical management. The pathological staging was reassessed with the new international tumor-node-metastasis staging system for EC approved by the American Joint Committee on Cancer (Version 9) (27). The specimens from 30 cases of EC were divided into the following groups based on the follow-up visits from 2019: i) Subjects with a good response and a survival of >3 years without recurrence (n=13), and subjects with a poor response, who died within 3 years due to recurrence (n=17); and ii) subjects without metastasis within 1 year after surgery (n=18), and subjects with metastasis within 1 year after surgery (n=12). All tissue specimens were paraffin-embedded for immunohistochemistry staining or stored in liquid nitrogen for immunoblotting and reverse transcription-quantitative (RT-qPCR) analysis. Ethical approval was obtained from the Medical Ethics Committee of Nanchong Central Hospital (approval no. 2019.095). The study protocol was carefully explained to the participants and participation was fully voluntary. Written informed consent was obtained from all participants and they agreed to the publication of their individual data.

Cell lines and cell culture. The human endometrial endothelial cell line, HEEC, and the human ESCC cell lines, EC109, KYSE-150, KYSE-510 and TE-3, were purchased from The Cell Bank of Type Culture Collection of The Chinese Academy of Sciences. The TE-3 cell line has been shown to be identical to the following cell lines: TE-2, TE-7, TE-12 and TE-13 (https://www.cellosaurus.org/CVCL_9971) (28,29). The EC109 cells used in the present study were authenticated using short tandem repeat analysis (Table SI). Cells were cultured in Dulbecco's Modified Eagle's Medium (Gibco; Thermo Fisher Scientific, Inc.) supplemented with 10% fetal bovine serum (AccuRef Scientific), 100 units/ml penicillin and 100 μg/ml streptomycin (Gibco; Thermo Fisher Scientific, Inc.). The cells were cultured under an atmosphere of 5% CO_2 at 37˚C. The concentration of nucleic acid was 20 nM and transfection was performed at room temperature, while subsequent experiments were conducted 48 h after transfection.

The KYSE-150 cells were transfected with an AGTR1-expressing pcDNA3.1 plasmid or empty vector (Thermo Fisher

Scientific, Inc.) or with AGTR1-targeting small interfering (si)RNA oligonucleotides (antisense strand, 5'-CUGUAG AAUUGCAGAUAUUdTdT-3' and sense strand, 3'-dTdTGA CAUCUUAACGUCUAUAA-5') or negative control (NC) oligonucleotides (antisense strand, 5'-UUCUCCGAACGU GUCACGUdTdT-3' and sense strand, 3'-dTdTAAGAGGCU UGCACAGUGCA-5') (Shanghai GenePharma Co., Ltd.). Cell transfection was performed using Lipofectamine 3000 reagent (Thermo Fisher Scientific, Inc.) following the manufacturer's instructions. After 48 h of transfection, cells were harvested for further analysis.

The Tet-on cell line with inducible expression of AGTR1 was constructed by transfection of KYSE-150 cells with the AGTR1-expressing pCDH plasmid (Vazyme Biotech Co., Ltd.) using Lipofectamine 3000 reagent as aforementioned and subsequent screening by limiting dilution cloning. AGTR1-expression was induced by treating the cells with 100 ng/ml doxycycline (MilliporeSigma). In some experiments, cells were treated with cisplatin (MilliporeSigma) at the indicated concentration and/or 5 μM fendiline (Thermo Scientific, Inc.) as specified.

Cell viability and colony formation assay. Cells were seeded in 96-well plates at a density of $5x10^3$ cells/well and incubated overnight. After the indicated treatments, Cell Counting Kit-8 reagent (AccuRef Scientific) was added to cells at the fixed time (24, 48 and 72 h) and the cells were incubated for another 2 h at 37˚C. The absorbance of each well was measured at 450 nm by a plate reader (SpectraMax iD3 Multi-Mode Microplate Reader; Molecular Devices LLC). The half maximal inhibitory concentration (IC_{50}) of cisplatin was calculated using GraphPad Prism (version 8.0; Dotmatics).

The colony forming ability of the cells was determined using a clonogenic assay. Briefly, cells were diluted and seeded in 12-well culture plates at a density of $1.5x10^4$ cells/well, and the cells were incubated at 37˚C under 5% CO_2 for 10 days. The cells were fixed with 4% paraformaldehyde (Biosharp Life Sciences) at room temperature for 30 min, then stained with Diff-Quik stain set (Siemens Healthineers) at room temperature for 10 min, washed with PBS (Gibco; Thermo Fisher Scientific, Inc.) to remove the stain that did not bind to the cells, imaged using a light microscope (Eclipse-TS100; Nikon Corporation) and counted using ImageJ software (version 1.53; National Institutes of Health). A cell cluster with >10 cells was considered to be a single colony.

Transwell migration and invasion assays. Transwell Boyden chambers (BD Biosciences) with 8-μm pore polycarbonate filters were used for *in vitro* cell migration assays, and chambers pre-coated with Matrigel (BD Biosciences) at 37˚C for 2 h were used to evaluate the *in vitro* invasive potential of EC cells. Briefly, cells were seeded at a density of $1x10^5$ per well in DMEM serum-free culture medium (Gibco; Thermo Fisher Scientific, Inc.) into the upper chamber that was coated with Matrigel (BD Biosciences) and 600 μl complete medium was added to the lower chamber. Chambers were then incubated for 24 h at 37˚C. At the time of harvesting, cells remaining inside the upper chambers were removed, while migrated and invaded cells on the lower surface of the membrane were fixed in 4% paraformaldehyde for 20 min and stained with crystal violet (MilliporeSigma) for 5 min (both at room temperature), followed by visualization and counting under an inverted microscope. Cells were imaged, and five visual fields per well were randomly selected for cell counting using ImageJ software (version 1.53; National Institutes of Health).

Wound healing assay. Cells were seeded in a 6-well plate at a concentration of $1x10^6$ cells per well, then cultured overnight to allow adequate adherence to form a confluent monolayer. The cell layers were wounded using a sterile 200 μl pipette tip and washed with serum-free medium to eliminate dislodged cells. Cells were imaged immediately (time 0 h) using an inverted microscope and then cultured with serum-free medium for 24 h. The wounds were imaged at 24 h post wounding to monitor the wound closure progression. The wound healing rate was calculated as follows: Wound healing rate (%)=[1-(24 h scratch width/0 h scratch width)] x100%. The wound closure distance of three independent wounds in each group was measured using ImageJ software (version 1.53; National Institutes of Health).

RT-qPCR. Total RNA was extracted from cells or tumor tissues using a High Pure RNA isolation kit (Roche Diagnostics) following the manufacturer's instructions. The RNA concentration was measured using a Nano Drop ONE spectrophotometer (Thermo Fisher Scientific, Inc.). RT was carried out on 1 μg of RNA using the SuperScript III RT kit with random hexamer primer (Thermo Fisher Scientific, Inc.) per the manufacturer's instructions. qPCR was then performed using SYBR Green reaction mix (AccuRef Scientific) and a 7500 Real-Time PCR System instrument (Thermo Fisher Scientific, Inc.) with the following conditions: 95˚C for 10 min and 40 cycles of 95˚C for 10 sec, 58˚C for 20 sec and 72˚C for 15 sec. The specific primer sequences were as follows: ATGR1, forward: 5'-CGGGGCGCGGGTTTG-3' and revers: 5'-TCAAATACACCTGGTGCCGA-3'; and β-actin, forward: 5'-TTCCTGGGCATGGAGTCC-3' and revers: 5'-CTCGTT ACTAGAACTAGAAGT-3'. The comparative threshold cycles (Cq) of tested mRNA and GAPDH were measured and their difference (ΔCq) was calculated. The relative expression was then calculated by the $2^{-\Delta\Delta Cq}$ method (30) with normalization to the control sample.

Western blotting. Cells or tissue specimens were lysed using RIPA buffer (AccuRef Scientific) supplemented with protease inhibitor cocktail (AccuRef Scientific). The protein content was determined by BCA Protein Assay Kit (AccuRef Scientific). A total of 40 μg protein was separated by 8% SDS-PAGE and then transferred to polyvinylidene difluoride membranes (MilliporeSigma). The membranes were blocked with 5% milk/PBS with Tween-20 (PBST; PBS:Tween, 1,000:1) for 1 h at room temperature and probed with antibodies against the targets overnight at 4˚C. After washing with PBST, the membranes were incubated with horseradish peroxidase-conjugated goat anti-rabbit IgG (H+L) (1:10,000; cat. no. SA00001-2; Proteintech Group, Inc.) or anti-mouse IgG (1:10,000; cat. no. SA00001-1; Proteintech Group, Inc.) as the secondary antibodies for 1 h at room temperature and then visualized by ECL detection kit (AccuRef Scientific). The band intensities of the proteins were analyzed using ImageJ

(version 1.53) densitometry software (National Institutes of Health). The primary antibodies used for the western blot assays are listed in Table SII.

Apoptosis assays. Apoptosis of EC cells was determined by Annexin V-FITC/propidium iodide (PI) double staining assay (AccuRef Scientific) according to the manufacturer's instructions. Apoptotic cells were counted with a FACSCalibur flow cytometer (BD Biosciences) and data were analyzed by FlowJo (version 10.8.1) software (BD Biosciences).

Paraffin-embedded cancer tissue was cut into slices of 4 μm thickness and then affixed to glass slides. The terminal deoxynucleotidyl transferase (TdT) dUTP nick-end labeling (TUNEL) assay was performed using a commercial TUNEL apoptosis assay kit (Beyotime Institute of Biotechnology). Briefly, cell or tissue slides were incubated with 2 μg/ml proteinase K (MilliporeSigma) in 10 mM Tris-HCl (pH 7.4) buffer containing 5 mM EDTA. Then, endogenous peroxidase was inactivated using 0.3% hydrogen peroxide for 20 min at room temperature. After washing with PBS three times, the slides were incubated with TUNEL solution (2 μl TdT + 48 μl fluorescent labelling solution) at 37˚C for 1 h in the dark. The slides were washed with PBS three times and then mounted with mounting medium containing DAPI (Vector laboratories, Inc.). Finally, the staining results were examined using a fluorescence microscope (DM1,000; Leica Microsystems GmbH), then five fields were randomly selected and the TUNEL-positive cells were calculated using ImageJ (version 1.53) software (National Institutes of Health).

Flow cytometry and ATP measurement. Cells were loaded with 1 μM Fluo-3, AM (Thermo Fisher Scientific, Inc.) in phenol red-free culture medium at 37˚C for 30 min following the manufacturer's protocol. After washing with PBS, KYSE-150 cells were kept in culture medium without phenol red. The intensity of fluorescent signal was measured with a FACSCalibur flow cytometer (BD Biosciences). The mitochondrial membrane potential of EC cells was measured by staining with 5,50,6,60-tetrachloro-1,10,3,30-tetraethyl-imidacarbocyanine iodide (JC-1; MillipreSigma) at a final concentration of 2.5 μM. After shaking in the dark at 37˚C for 15 min, the cells were analyzed using a FACSCalibur flow cytometer (BD Biosciences). Flow cytometry data were analyzed with the FlowJo (v10.8.1) software (BD Biosciences). The ATP levels were measured with the Molecular Probes® ATP Determination Kit (Thermo Fisher Scientific, Inc.) following the manufacturer's protocol.

Immunohistochemistry staining. After dissection, the tumor tissues were mounted in paraffin embedding compound and frozen at -80˚C. The cryostat sections were prepared by cutting the tissues at a thickness of 5 μm using a cryostat microtome (Leica Microsystems GmbH). The tumor tissues were soaked in xylene three times for 3-5 min each, with new xylene added each time. Tissues were dehydrated in anhydrous ethanol twice for 3-5 min each. Tissues were incubated with 95% ethanol for 3-5 min, 90% ethanol for 3-5 min and 70% ethanol for 3-5 min. The tissues were rinsed twice with distilled water for 3-5 min each. Subsequently, the tissues were soaked in antigen retrieval solution (1X) and heated at 96˚C for ~20 min in a water bath. The slides were fixed in 4% formalin solution for 10 min at 37˚C and washed with PBS three times. An appropriate amount of endogenous peroxidase blocking solution (undiluted; cat. no. P0100A; Beyotime Institute of Biotechnology) was added dropwise to completely cover the sample, and the samples were incubated at room temperature for 5-10 min or 37˚C for 5 min. The slides were then incubated with PBS containing 0.1% Triton X-100 for 10 min and washed in PBS three times. Next, the slides were incubated with 10% goat serum (cat. no. ZLI-9022; Beijing Zhongshan Jinqiao Biotechnology Co., Ltd.) in PBST (0.1% Tween 20) for 30 min at room temperature to block the unspecific binding of the antibodies. After incubation with the primary antibodies against AGTR1 (2.5 μg/ml dilution; cat. no. 124505; Abcam) or Ki-67 (2.5 μg/ml; cat. no. ab15580; Abcam) overnight at 4˚C, the slides were washed three times in PBST and then incubated with biotinylated secondary antibody (1:200; cat. no. PV-9005; Beijing Zhongshan Jinqiao Biotechnology Co., Ltd.) at room temperature for 30 min. The signal was then visualized using the DAB method (AccuRef Scientific) according to the manufacturer's protocol. Next, the slides were counterstained with hematoxylin (Nanjing Jiancheng Bioengineering Institute) for 20 sec at room temperature to visualize the nuclei. After mounting with mounting medium, the slides were imaged using a light microscope with x20 and x40 objective (NA1.3; Leica Microsystems GmbH) and analyzed using GraphPad Prism (version 8.0; Dotmatics).

Animal experiments. Female athymic mice (BALB/c, nu/nu; 15-20 g; 6-8 weeks old) were purchased from Charles River Laboratories, Inc., and housed at the specific pathogen-free facility at the Animal Center of North Sichuan Medical College (Nanchong, China). The mice were maintained at room temperature (22±1˚C) with a 12/12 h light/dark cycle and *ad libitum* access to food and water. The indicated KYSE-150 cell lines or EC109 cell lines were injected subcutaneously into the right flank of each mouse (100 μl; $1x10^6$ cells/mouse) to establish the xenograft model (20 mice per experiment for 4 groups for 2 experiments; 5 mice in each group). Mice were divided into the following eight groups: pEmpty, pAGTR1, pEMPty + cisplatin, pAGTR1 + cisplatin; or cisplatin, cisplatin + Dox, cisplatin + fendiline and cisplatin + fendiline + Dox, as indicated. In some experiments, mice received treatments, alone or in combination as indicated, including intraperitoneal injection of the vehicle PBS or cisplatin at a dose of 5 mg/kg body weight twice every week, intraperitoneal injection of Dox at a dose of 20 mg/kg body weight every other day and gastric gavage administration of fendiline at a dose of 3 mg/kg body weight every other day. All treatments began when the tumor mass reached a diameter of 5 mm. Tumor size was measured once a week with calipers and tumor volumes were calculated by the following formula: $length^2$ x width x $\pi/6$. Animals were checked daily, and any animal found unexpectedly to be moribund, cachectic or unable to obtain food or water was euthanized. In addition, mice with a tumor burden exceeding 2 cm diameter in any direction or a tumor volume >4.2 cm^3 were euthanized. None of the mice reached the humane endpoints in the present study.

In total, 5 weeks after the initiation of treatments, mice were euthanized (no animals were found dead in this study)

and tumor tissues were subjected to further analyses. Animals were euthanized using a 30-70% per min displacement of chamber air with compressed CO_2. After the completion of euthanasia with CO_2 inhalation, cervical dislocation with the confirmation of a gap between the skull and spinal column was used to verify the death of mice. All tumors were resected from mice and the total tumor weight in each mouse was measured. Some tumors were fixed in 10% formalin for 24 h at room temperature for subsequent immunohistochemistry. Animal experiments were conducted in accordance with the procedures and protocols of the Animal Center of North Sichuan Medical College and approved by the Ethics Committee of North Sichuan Medical College (approval no. NSMC202144).

RNA sequencing (RNA-seq) and bioinformatics. RNA was isolated from EC tumor and normal esophageal tissues using the RNeasy Kit (cat. no. 74104; Qiagen GmbH) according to the manufacturer's instructions. The integrity of total RNA in samples was detected by 2% agarose gel electrophoresis, and a NanoDrop (ND-1,000; Thermo Fisher Scientific, Inc.) was used for quantification and further quality inspection. For each sample, 1-2 μg total RNA was selected for sequencing library construction. The total RNA was enriched with the NEBNext Poly (a) mRNA Magnetic Isolation Module (cat. no. E7490S; New England BioLabs, Inc.). After treatment, the RNA library was constructed with a KAPA Stranded RNA-seq Library Prep Kit (cat. no. KK8401; Illumina, Inc.). The KAPA kit used the construction method of a chain-specific library based on dUTP. The constructed library was inspected using an Agilent 2100 Bioanalyzer (library concentration, fragment size 400-600 bp and whether there were connectors), and the library was finally quantified by qPCR. For qPCR, DNA was extracted using Qiagen DNeasy Blood & Tissue kit (Qiagen GmbH) and the reaction was performed using Phusion High-Fidelity DNA Polymerase (Thermo Fisher Scientific, Inc.). The random PCR primers, which were used for cDNA synthesis followed by PCR amplification, were as follows: Forward, 5'-AGTACCGTACGATGACT-3' and reverse, 5'-CAG TGCATAGTACAGTC-3'. The thermocycling conditions were as follows: Initial denaturation at 95˚C for 3 min, followed by denaturation at 95˚C for 30 sec, annealing at 55˚C for 30 sec and extension at 72˚C for 1 min (35 cycles); final extension at 72˚C for 5-10 min; hold at 4˚C indefinitely. PCR products were analyzed using a 1.5% agarose gel and visualized using SYBR Green. According to the quantitative results and the amount of final sequencing data, the sequencing libraries of different samples were required to be mixed in the sequencing process. The mixed sequencing libraries of different samples were denatured with 0.1 M NaOH to generate single-stranded DNA, diluted to 8 pM, and then amplified *in situ* using a Truseq SR Cluster Kit (cat. no. GD-401-3001; Illumina, Inc.). The ends of the generated fragments were sequenced using an Illumina HiSeq2000™ Genome Analyzer (Illumina, Inc.). Reference-based RNA-seq was performed with a nucleotide length of 200-400 bp. The direction of sequencing was forward and reverse strands. The loading concentration of the final library was 10 nM, which was determined using a Qubit fluorometer (Thermo Fisher Scientific, Inc).

Solexa Pipelime (Off Line Base Caller software; version 1.8; Illumina, Inc) was used for image processing and base recognition. FastQc software (version 0.11.6; Babraham Bioinformatics) was used to evaluate the sequencing quality of reads. Sequences were aligned to the reference genome using Hisat software (version 2.2.1; https://daehwankimlab.github.io/hisat2/). StringTie software (version 2.2.0; https://ccb.jhu.edu/software/stringtie/) was employed to estimate transcriptional abundance by referencing official database annotation information. R software (version 4.1.2; https://cloud.r-project.org/bin/windows/) was used to perform fragments per kilobase of transcript per million mapped reads calculations at the gene and transcript levels, and to calculate the expression differences at both the gene and transcript levels. Differentially expressed genes were selected between samples or groups. RNA-sequencing data were uploaded to the publicly available Gene Expression Omnibus (GEO) database with the accession number GSE263647 (https://www.ncbi.nlm.nih.gov/geo/query/acc.cgi?acc=GSE263647).

The differentially expressed genes were determined using a false discovery rate of <5% and a fold change >1.5. The ENCODE project database (www.encodeproject.org) was utilized to search for the most enriched Kyoto Encyclopedia of Genes and Genomes pathways in the selected gene lists. In addition, the Database for Annotation, Visualization, and Integrated Discovery (https://davidbioinformatics.nih.gov/) was employed to search for the most enriched biological processes, molecular functions and cellular component terms of the Gene Ontology. Enrichment scores were used to indicate the enrichment level of genes assigned to the indicated Gene Ontology terms in each subgroup. Related pathways were evaluated by Gene Set Enrichment Analysis. To perform expression analysis, pan-cancer was selected on the home page (https://starbase.sysu.edu.cn/; version 3.0) to enter the gene differential expression and survival analysis platform, and AGTR1 was compared between cancer and normal samples. The conditions set for the Kmplot online website (https://kmplot.com/analysis/) were: Matching The Cancer Genome Atlas dataset (RNA-seq pan-cancer); stage, all; sex, all; ethnicity, all; grade, all; follow-up threshold, all; and cutoff value used in the analysis, 10. Overall survival and metastasis-free survival in patients with EC were computed with the Kaplan-Meier method, and the log rank test was used to assess the statistical significance of the results.

Statistical analysis. Data are presented as the mean ± standard deviation. The differences between two groups were analyzed by unpaired Student's t-test. ANOVA with Bonferroni correction was applied to compare the differences between more than two groups. All statistical analyses were performed with GraphPad Prism (version 8.0; Dotmatics) software. $P<0.05$ was considered to indicate a statistically significant difference.

Results

Expression of AGTR1 is downregulated in recurrent and metastasized EC tissues. To explore the genes that are potentially associated with the progression of EC, RNA-seq was performed using EC and normal esophageal tissues. As shown in the volcano plot of Fig. 1A, RNA-seq analysis demonstrated that 969 genes were differentially downregulated, while 1,408 genes were significantly upregulated in EC tissues

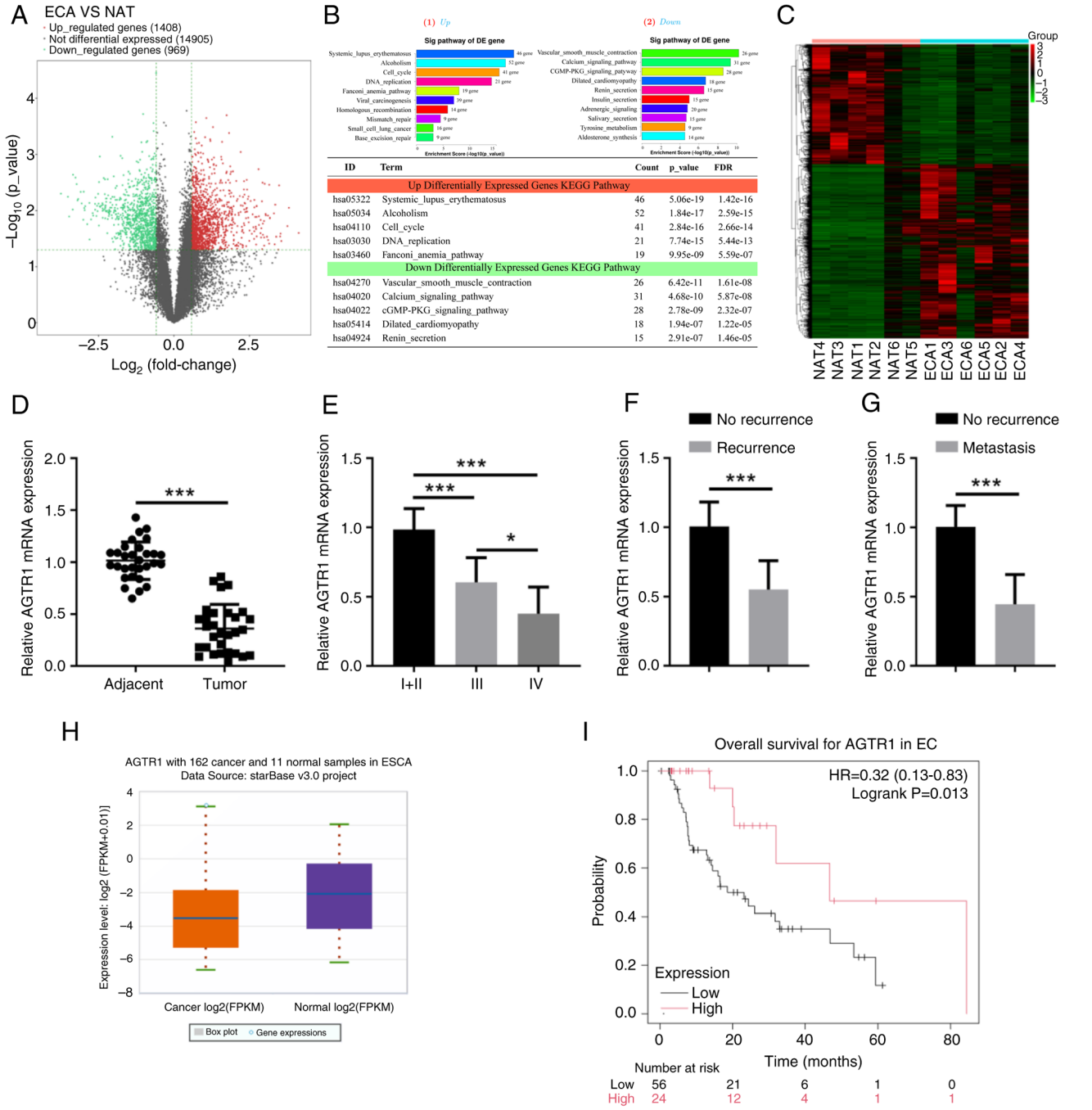

Figure 1. EC tissues have lower AGTR1 expression, which is a prognostic marker in recurrent and metastasized EC. (A) ECA (n=5) and NAT (n=5) were subjected to RNA-sequencing analyses, and the DE genes were plotted in a Volcano Plot. (B) The top 10 significantly changed signaling pathways involving the DE genes are shown. (C) The heatmap shows the expression levels of 31 genes in the calcium signaling pathway. (D) The mRNA levels of AGTR1 in adjacent normal tissues (n=30) and EC tumor tissues (n=30) were determined by RT-qPCR. Relative mRNA levels of AGTR1 in tumor samples from patients at (E) stages I/II (n=14), III (n=9) and IV (n=7), (F) without (n=13) or with recurrence (n=17) or (G) without (n=18) or with metastasis (n=12), were determined by RT-qPCR. Bioinformatics analyses showing (H) AGTR1 expression and (I) overall survival of patients with EC. Data were retrieved from starbase (https://starbase.sysu.edu.cn/; https://kmplot.com/analysis/). *P<0.05, ***P<0.001. ESCA, esophageal carcinoma; EC, esophageal cancer; ECA, EC tumor tissues; NAT, normal esophageal tissues; DE, differentially expressed; RT-qPCR, reverse transcription-quantitative PCR; AGTR1, angiotensin II receptor type 1.

compared with the normal tissues. Related pathways analysis showed that the 'calcium signaling pathway' was among the top significantly enriched pathways (Fig. 1B), and the heatmap data indicated that most of the genes in the calcium signaling pathway had downregulated expression in EC tissues compared with normal tissues (Fig. 1C). AGTR1, a significantly downregulated gene, became the subject focus, and the qPCR results in a validation cohort of samples confirmed that the AGTR1 mRNA level in EC tissues was significantly lower than that in adjacent normal esophageal tissues (Fig. 1D). The expression of AGTR1 and the disease progression of EC was further investigated and it was found that patients at the later development stages (Fig. 1E), with cancer recurrence after cisplatin treatments (Fig. 1F) or with cancer metastasis (Fig. 1G) had significantly reduced expression levels of AGTR1. Moreover, the data mining of public databases (starBase) also revealed a

lower AGTR1 expression level in tumor tissues compared with normal tissues (Fig. 1H), and that patients with a high AGTR1 expression level showed improved overall survival (Fig. 1I). Taken together, these results suggest that AGTR1 may be a prognostic marker, the expression of which is downregulated in recurrent and metastasized EC.

AGTR1 expression increases chemosensitivity of EC cells to cisplatin in vitro and in vivo. To investigate the biological effect of AGTR1 on the development of EC, the expression of AGTR1 in EC cell lines was first evaluated. Compared with the control HEECs, the EC cell lines (including KYSE-150, KYSE-510 and TE-3) showed significantly downregulated expression of AGTR1 mRNA (Fig. 2A) and protein (Fig. 2B). Following this, the cisplatin IC_{50} values of the tested EC cell lines were determined. Notably, KYSE-150 cells with the lowest AGTR1 expression had the largest IC_{50} value, while EC109 cells with a higher AGTR1 expression displayed a smaller IC_{50} value (Fig. 2C). To further confirm the roles of AGTR1 expression in sensitizing EC cells to cisplatin, the impacts on cell viability and colony formation in response to cisplatin treatments in KYSE-150 cells and EC109 cells after AGTR1 ectopic expression and knockdown, respectively, were examined. Overexpression of AGTR1 in KYSE-150 cells (Fig. 2D and E) significantly reduced the cell viability upon treatment with cisplatin at various concentrations (Fig. 2F), which was accompanied by reduced colony-formation (Fig. 2G). On the contrary, knockdown of AGTR1 in EC109 cells (Fig. 2H and 2I) significantly increased cell viability (Fig. 2J) and the colony formation ability (Fig. 2K) in response to cisplatin treatment.

Animal experiments were further conducted with xenografted EC cells to consolidate the chemosensitivity-promoting role of AGTR1 expression *in vivo*. The growth of engrafted control KYSE-150 cells and AGTR1-overexpressing KYSE-150 cells were compared upon *in vivo* cisplatin therapy in nude mice (Fig. 3A). Compared with the control group without treatments, cisplatin administration reduced the tumor volume and weight and a higher reduction was observed in the AGTR1-overexpressing group (Fig. 3B and C). This trend was in-line with the lowest cell proliferation as revealed by Ki-67 IHC (Fig. 3D) and highest level of apoptosis shown by TUNEL staining (Fig. 3E and F) in the cisplatin-treated AGTR1-overexpressing group. Furthermore, the protein level of N-cadherin and Vimentin in the AGTR1-overexpressing group, the cisplatin group and the cisplatin-treated AGTR1-overexpressing group were decreased, while the protein level of E-cadherin was increased (Fig. 3G).

Additionally, how AGTR1 knockdown impacted the growth of engrafted EC109 cells in nude mice upon cisplatin administration was also tested (Fig. S1A). Consistently, EC109 cells with AGTR1 knockdown grew larger than the control cells in mice with or without cisplatin treatments (Fig. S1B and C), which was accompanied by increased Ki-67 staining (Fig. S1D) and reduced apoptosis in tumor tissues (Fig. S1E and F). In addition, the protein levels of N-cadherin and Vimentin in the AGTR1 knockdown group were increased and the protein level of E-cadherin was decreased. However, cisplatin decreased the protein level of N-cadherin and Vimentin, and increased the protein level of E-cadherin in both control and AGTR1-konckdown cells (Fig. S1G). Therefore, these *in vitro* and *in vivo* studies demonstrated that AGTR1 expression increased the chemosensitivity of EC cells to cisplatin.

AGTR1 expression and cisplatin administration affects the metastasis-relevant traits of EC cells. Since a higher expression level of AGTR1 was found in patients with EC without metastasis (Fig, 1G), the potential role of AGTR1 in suppressing metastasis of EC cells was next evaluated. Transwell experiments were performed using control KYSE-150 cells, AGTR1-overexpressing KYSE-150 cells, cisplatin-treated AGTR1-overexpressing KYSE-150 cells, control EC109 cells, AGTR1-knockdown EC109 cells and cisplatin-treated AGTR1-knock down EC109 cells. As shown in Fig. 4A, ectopic expression of AGTR1 or cisplatin administration caused the significantly reduced migration and invasion of KYSE-150 cells. In line with this observation, EC109 cells with AGTR1 knockdown had significantly enhanced migration and invasion (Fig. 4B), compared with the control EC109 cells. As expected, the wound healing assay demonstrated similar trends. Compared with the control KYSE-150 cells, AGTR1 overexpression or cisplatin administration significantly diminished the wound healing ability (Fig. 4C, upper). Consistently, AGTR1 knockdown in EC109 cells resulted in enhanced wound healing ability (Fig. 4C, lower).

To unravel the molecular mechanisms underlying the chemo-sensitizing roles of AGTR1 expression, the relationship between AGTR1 expression and intracellular calcium level in EC cells were further evaluated. AGTR1 overexpression in KYSE-150 cells enhanced the intracellular Ca^{2+} levels (Figs. 4D and S2A), while the AGTR1 knockdown in EC109 cells reduced the intracellular Ca^{2+} levels (Figs. 4E and S2A). Notably, AGTR1 overexpression in KYSE-150 cells enhanced the apoptosis rate (Figs. 4F and S2B), while the AGTR1 knockdown in EC109 cells reduced the apoptosis rate (Figs. 4G and S2B). Furthermore, the protein level of N-cadherin and Vimentin in the AGTR1-overexpressing group, the cisplatin group and the cisplatin-treated AGTR1-overexpressing group were decreased, while the protein level of E-cadherin was increased (Fig. 4H). However, the protein level of N-cadherin and Vimentin in the AGTR1 knockdown group were increased and the protein level of E-cadherin was decreased. However, cisplatin reduced the protein levels of N-cadherin and Vimentin, while increasing the protein content of E-cadherin in both control and AGTR1-konckdown cells (Fig. 4I). Collectively, these data indicate that AGTR1 expression affects metastasis-relevant traits in EC cells.

AGTR1 expression upregulates intracellular Ca^{2+} levels and enhances mitochondria-dependent apoptosis in EC cells. To verify the pro-apoptosis role of high intracellular Ca^{2+} levels in EC cells, the cells were treated with fendiline, which is a non-selective calcium channel blocker and causes accumulation of Ca^{2+} in cells. First, it was confirmed that the intracellular Ca^{2+} levels in fendiline-treated cells were much higher than the corresponding control cells (Figs. 5A and S2C), which were accompanied by a reversed trend in ATP levels (Fig. 5B) and a similar trend in mitochondrial membrane potential loss,

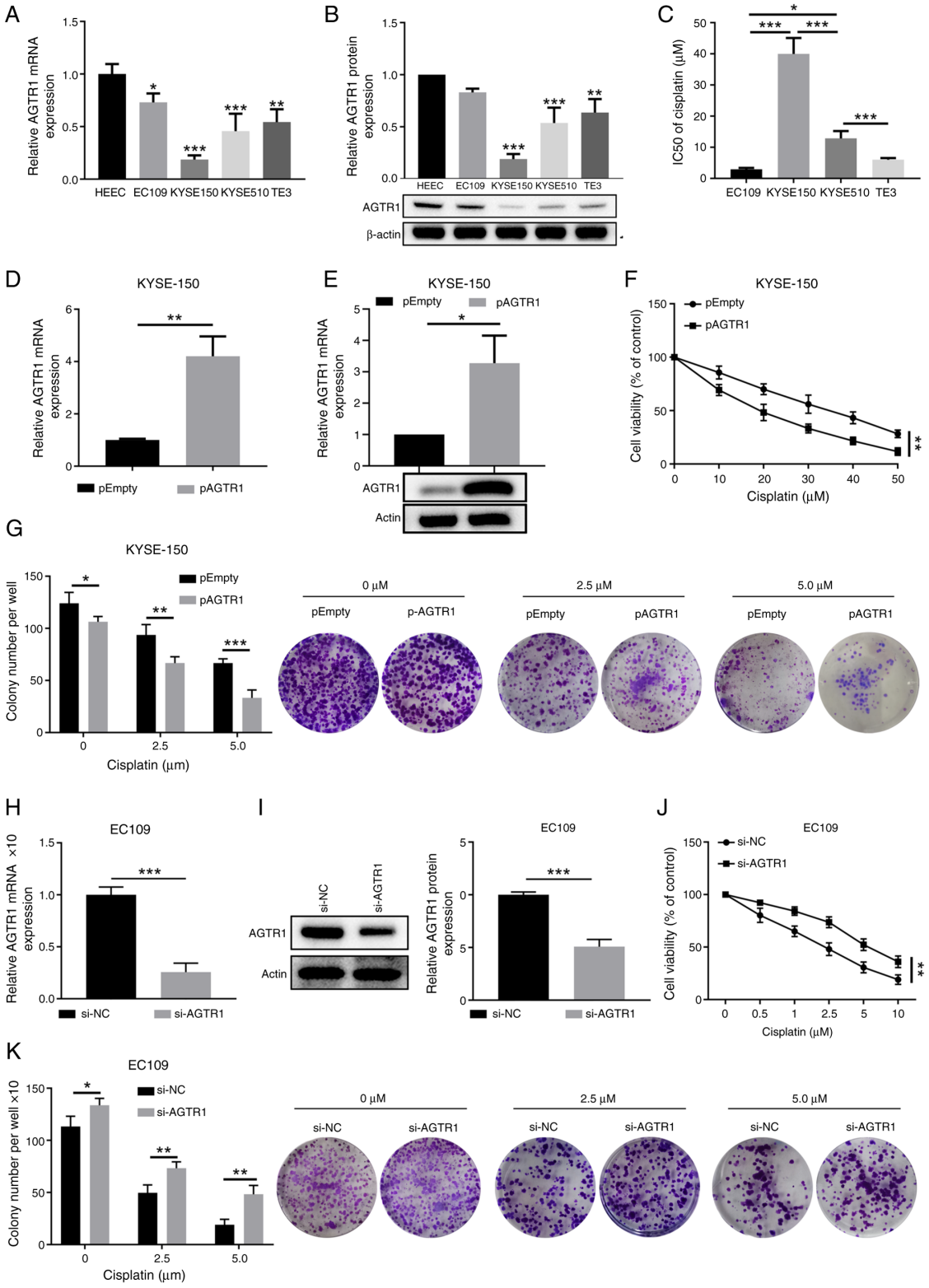

Figure 2. AGTR1 expression in EC tumors promotes the chemosensitivity to cisplatin *in vitro*. (A) The mRNA and (B) protein levels of AGTR1 in control HEECs and selected EC cell lines (EC109, KYSE-150, KYSE-510 and TE-3) were quantitated by RT-qPCR and western blotting, respectively. Representative images of western blot bands are shown. (C) IC_{50} values for cisplatin in selected EC cell lines were compared. Cells were treated with cisplatin at a range of concentrations (0-50 μM) for 72 h and IC_{50} was calculated. KYSE-150 cells were transfected with empty vector plasmid or AGTR1-overexpressing plasmid. After 48 h of transfection, the expression of AGTR1 (D) mRNA was determined by RT-qPCR and (E) protein was determined by western blotting. (F) Viability of control and AGTR1-overexpressing KYSE-150 cells treated with cisplatin at the indicated doses was measured by CCK-8 assays. Control group, pEmpty (0 μM). (G) Colony formation ability of control and AGTR1-overexpressing KYSE-150 cells upon treatment with cisplatin at the indicated doses was determined. Representative images of colony formation are shown, and colony numbers per well were summarized. EC109 cells were transfected with NC or AGTR1-specific siRNA oligos. After 48 h of transfection, the expression of AGTR1 (H) mRNA was determined by RT-qPCR and (I) protein was determined by western blotting. The (J) viability and (K) colony formation ability of EC109 cells upon treatment with cisplatin at the indicated concentrations were measured by CCK-8 and colony-formation assays, respectively. n=3 for each group. Control group, si-NC (0 μM). (G and K) Magnification, x10. *P<0.05, **P<0.01, ***P<0.001. EC, esophageal cancer; AGTR1, angiotensin II receptor type 1; HEEC, human esophageal epithelial cell; RT-qPCR, reverse transcription-quantitative PCR; CCK-8, Cell Counting Kit-8; NC, negative control; siRNA, small interfering RNA.

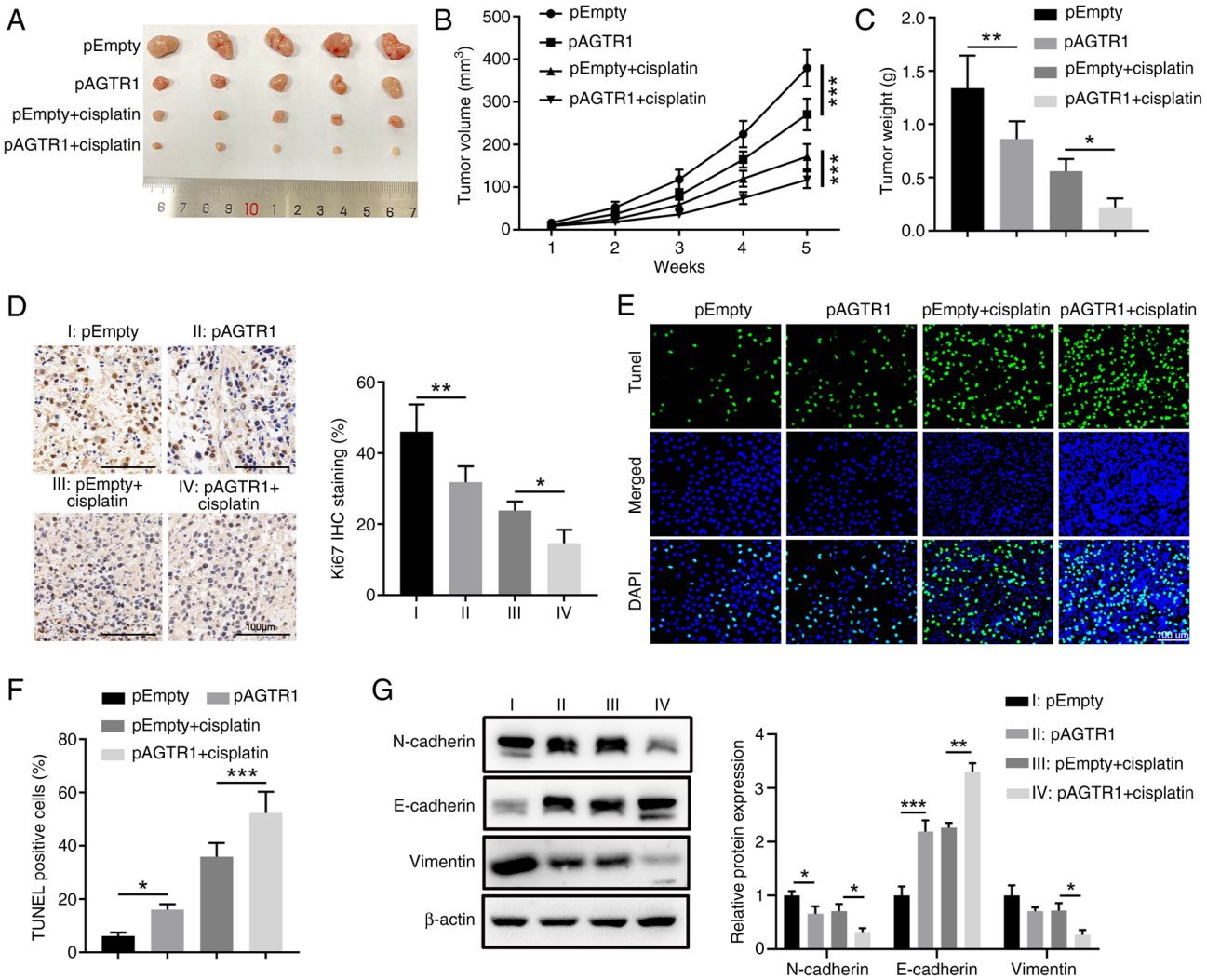

Figure 3. AGTR1 expression increases the chemosensitivity of KYSE-150 EC cells to cisplatin *in vivo*. Control and AGTR1-overexpressimg KYSE-150 cells were injected subcutaneously into the right flank of nude mice ($1x10^6$ cells/mouse) to establish the xenograft model. Mice were treated with an intraperitoneal injection of vehicle (PBS) or cisplatin (5 mg/kg body weight) twice every week. Tumor volume was monitored once per week and tumor tissues were collected at 36 days after tumor inoculation. (A) Tumor images of the indicated four groups. (B) Tumor growth curves and (C) weight at the end time point. (D) Cell proliferation in tumor tissues was evaluated by Ki-67 staining. Representative IHC images are shown and the Ki-67 staining intensity was semi-quantified using ImageJ software. (E) Apoptosis of tumor tissues was quantitated by TUNEL staining. Representative images are shown and (F) the percentage of $TUNEL^+$ cells are summarized. (G) The protein level of N-cadherin, E-cadherin and Vimentin were detected by western blotting. n=5 for each group. $^*P<0.05$, $^{**}P<0.01$, $^{***}P<0.001$. IHC, immunohistochemistry; TUNEL, terminal deoxynucleotidyl transferase dUTP nick-end labeling; AGTR1, angiotensin II receptor type 1.

as indicated by JC-1 staining (Fig. 5C). Moreover, additional fendiline treatments caused higher mitochondria-dependent apoptosis, as indicated by the increased protein expression levels of Bax, cleaved caspase 3/8/9, cleaved PARP and cytosolic cytochrome c, as well as decreased protein expression of Bcl-2 in KYSE-150 cells (Fig. 5D). Moreover, the impacts of fendiline treatment on control EC109 cells and AGTR1-knockdown EC109 cells were also evaluated. In agreement with that observed in KYSE-150 cells, fendiline treatments led to increased intracellular Ca^{2+} levels (Figs. S3A and S2D), decreased ATP levels (Fig. S3B), increased mitochondrial membrane potential loss (Fig. S3C) and increased mitochondria pathway-mediated apoptosis (Fig. S3D) in EC109 cells. Thus, these results indicate that upregulation of intracellular Ca^{2+} levels and enhanced mitochondria-dependent apoptosis are associated with the beneficial roles of AGTR1 expression in chemo-sensitizing EC cells.

AGTR1 expression and fendiline treatment-mediated increase in intracellular Ca^{2+} level contributes to chemosensitivity to cisplatin in EC cells. After the identification of increased intracellular Ca^{2+} levels as an underlying mechanism in mediating the AGTR1 expression-induced tumor suppressive effects in EC cells, it was further evaluated whether this approach could be utilized to enhance the chemo-sensitivity of EC cells to cisplatin. First, the Tet-on KYSE-150 cell line was generated and it was confirmed that Dox successfully induced expression of AGTR1 (Figs. 6A and S4A). This KYSE-150 cell line was treated with cisplatin, alone or in the presence of fendiline or/and Dox. Compared with the group with cisplatin stimulation alone, fendiline treatment or AGTR1 overexpression induced by Dox significantly reduced cell proliferation. Notably, the group with the combinational treatments of both fendiline and Dox were significantly more reduced (Fig. 6B). Compared with cisplatin stimulation alone, combinational treatments of

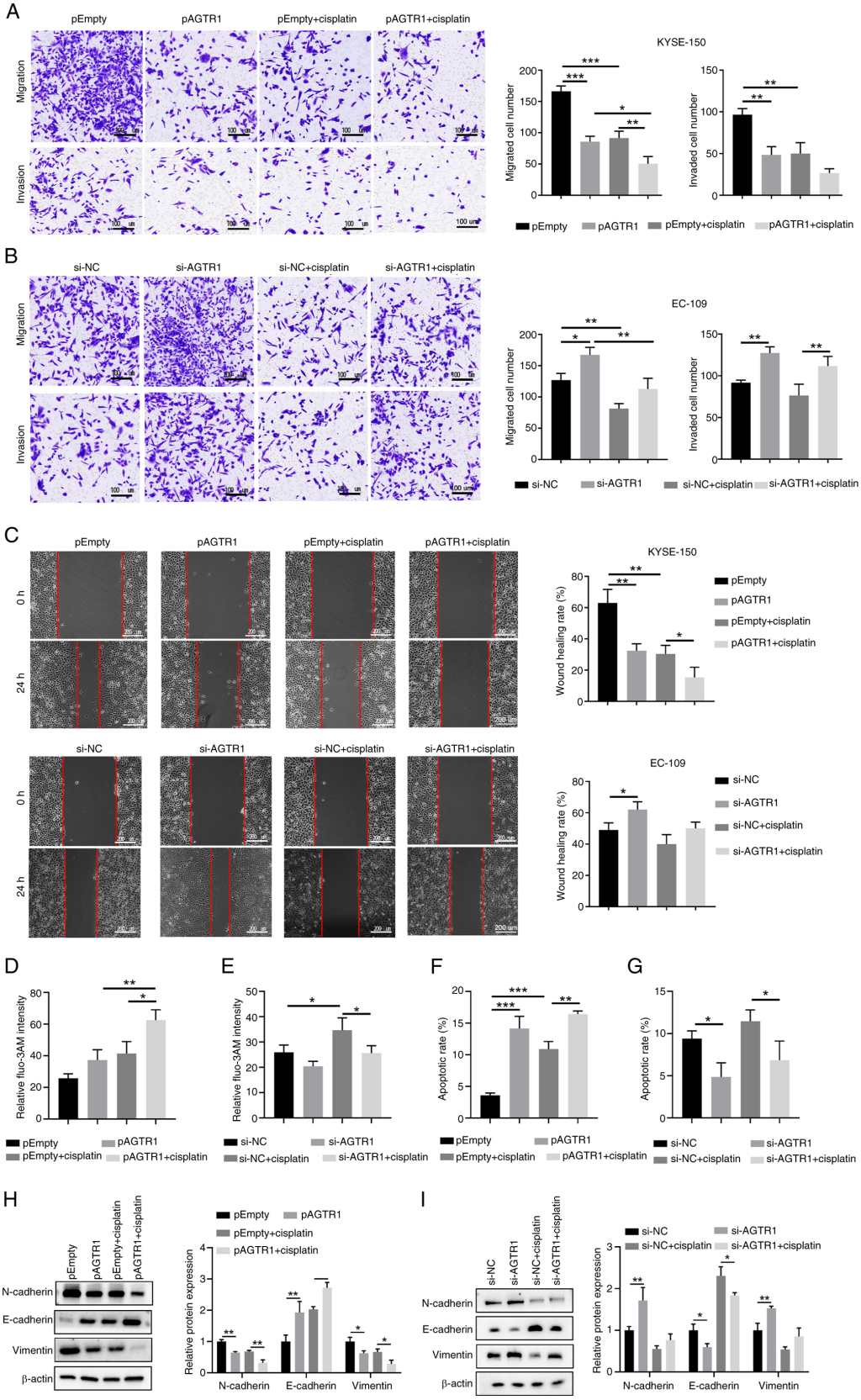

Figure 4. AGTR1 expression suppresses the metastasis-relevant traits of EC cells and upregulates intracellular Ca^{2+} levels as well as enhances mitochondria-dependent apoptosis *in vitro*. (A) Control, KYSE-150 cells with AGTR1 overexpression, cisplatin and cisplatin-treated AGTR1-overexpressing cells, in addition to (B) control, EC109 cells with AGTR1-knockdown, cisplatin and cisplatin-treated AGTR1 knockdown cells were subjected to Transwell assays. Representative images are shown and the migrated/invaded cells numbers were quantified. (C) Wound healing assays of the indicated EC cells. Wounds were imaged at 0 and 24 h following wound formation. Representative images are shown and the extent of wound closure was quantified. (D, E) The intracellular Ca^{2+} levels of the indicated eight groups were determined by flow cytometry with the calcium indicator, Fluo-3 AM. (F, G) The apoptosis of the indicated eight groups were determined by flow cytometry with Annexin V/PI staining. (H, I) The protein level of N-cadherin, E-cadherin and Vimentin of the indicated eight groups were detected by western blotting. n=5 for each group. *P<0.05, **P<0.01, ***P<0.001. EC, esophageal cancer; AGTR1, angiotensin II receptor type 1; NC, negative control; siRNA, small interfering RNA.

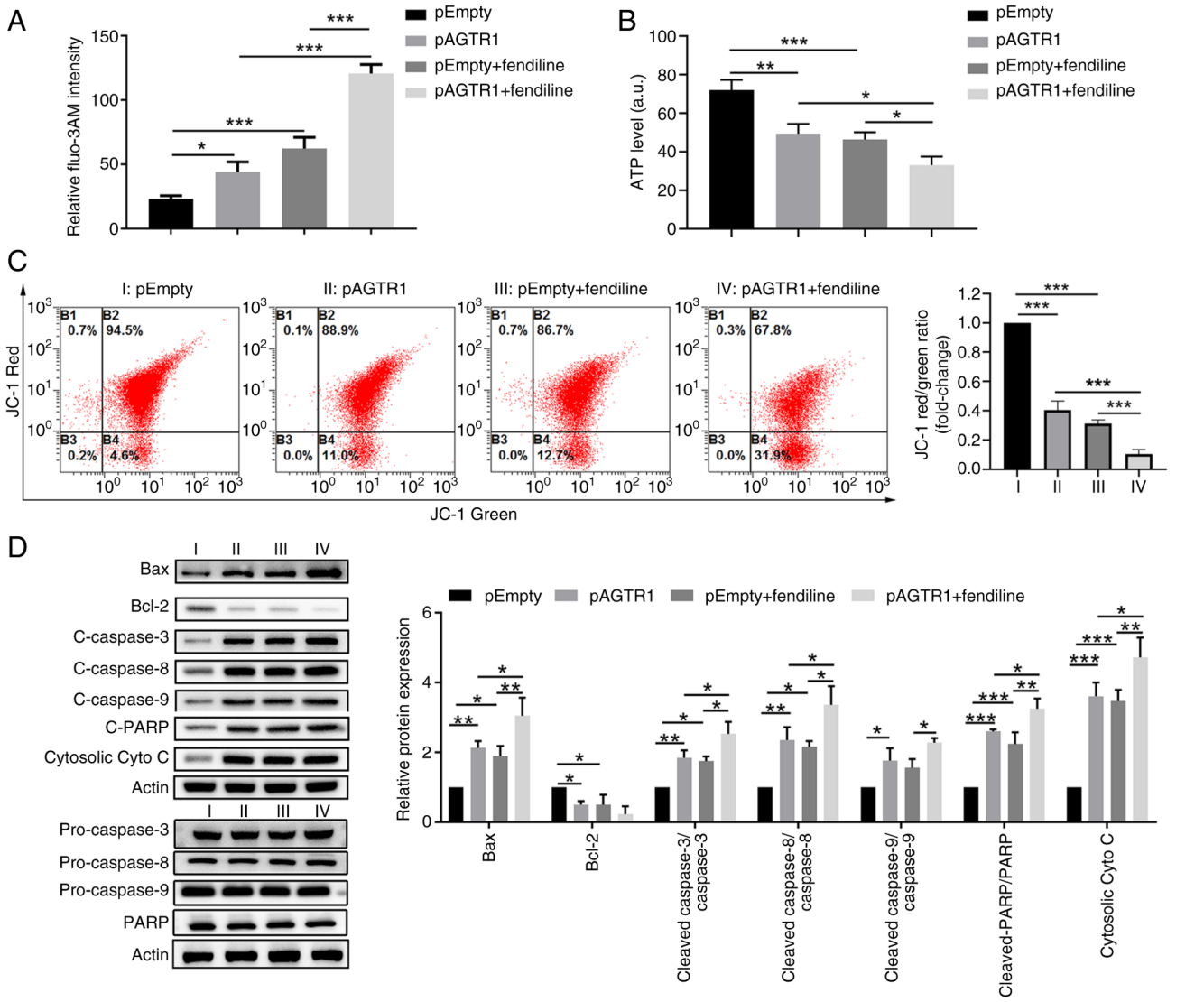

Figure 5. AGTR1 overexpression in KYSE-150 cells upregulates intracellular Ca^{2+} levels and enhances mitochondria-dependent apoptosis. KYSE-150 cells were transfected with empty plasmid or AGTR1-overexpressing plasmid and were treated with/without fendiline. (A) The intracellular Ca^{2+} levels were determined by flow cytometry with the calcium indicator, Fluo-3 AM. (B) The ATP levels were quantified. (C) The mitochondrial membrane potentials were analyzed by JC-1 staining and flow cytometry. (D) The levels of proteins involved in mitochondria pathway-dependent apoptosis were determined by western blotting. Representative images of the bands are shown. n=5 for each group. *P<0.05, **P<0.01, ***P<0.001. AGTR1, angiotensin II receptor type 1.

fendiline or Dox increased the intracellular Ca^{2+} level, as indicated by fluo-3AM staining (Figs. 6C and S4B), and the level of mitochondrial membrane potential loss, as measured by JC-1 staining (Figs. 6D and 6E). Moreover, the apoptosis rates indicated by Annexin V/PI staining (Figs. 6F and S4C) and the changes in mitochondrial apoptosis-related protein levels showed similar trends among the four groups (Fig. 6G), that is, compared with the cisplatin alone group, fendiline or Dox treatment increased apoptosis, while the group with concurrent fendiline and Dox administration displayed higher levels of apoptosis. It was also evaluated how fendiline impacted the metastasis-relevant traits in EC cells. Compared with the control Tet-on KYSE-150 cells without treatment, single fendiline or single Dox stimulation significantly reduced cell migration and invasion (Fig. 6H and I), as well as the wound healing ability of cells (Fig. 6J), while simultaneous administration of fendiline and Dox more notably reduced the metastasis-relevant traits of KYSE-150 cells. Taken together, these results suggest that the AGTR1 overexpression and fendiline treatment-mediated increase in intracellular Ca^{2+} level contributes to chemosensitivity to cisplatin in EC cells.

Xenograft animal model verifies the feasibility of using fendiline to potentiate the therapeutic efficacy of cisplatin in EC. To further clarify the beneficial effects of synchronous administration of fendiline and cisplatin in treating EC, a xenograft mice model was established by inoculating the Tet-on KYSE-150 cells into nude mice and treating them with cisplatin alone or together with fendiline or Dox or with both fendiline and Dox (Fig. 7A). Compared with the cisplatin treatment only group, either Dox administration-induced AGTR1 expression or fendiline exposure, significantly reduced the growth of engrafted EC cells, while simultaneous administration of fendiline and Dox inhibited tumor growth (Fig. 7B). This was also evidenced by the lowest tumor weight among the four groups at the end time-point (Fig. 7C). In agreement

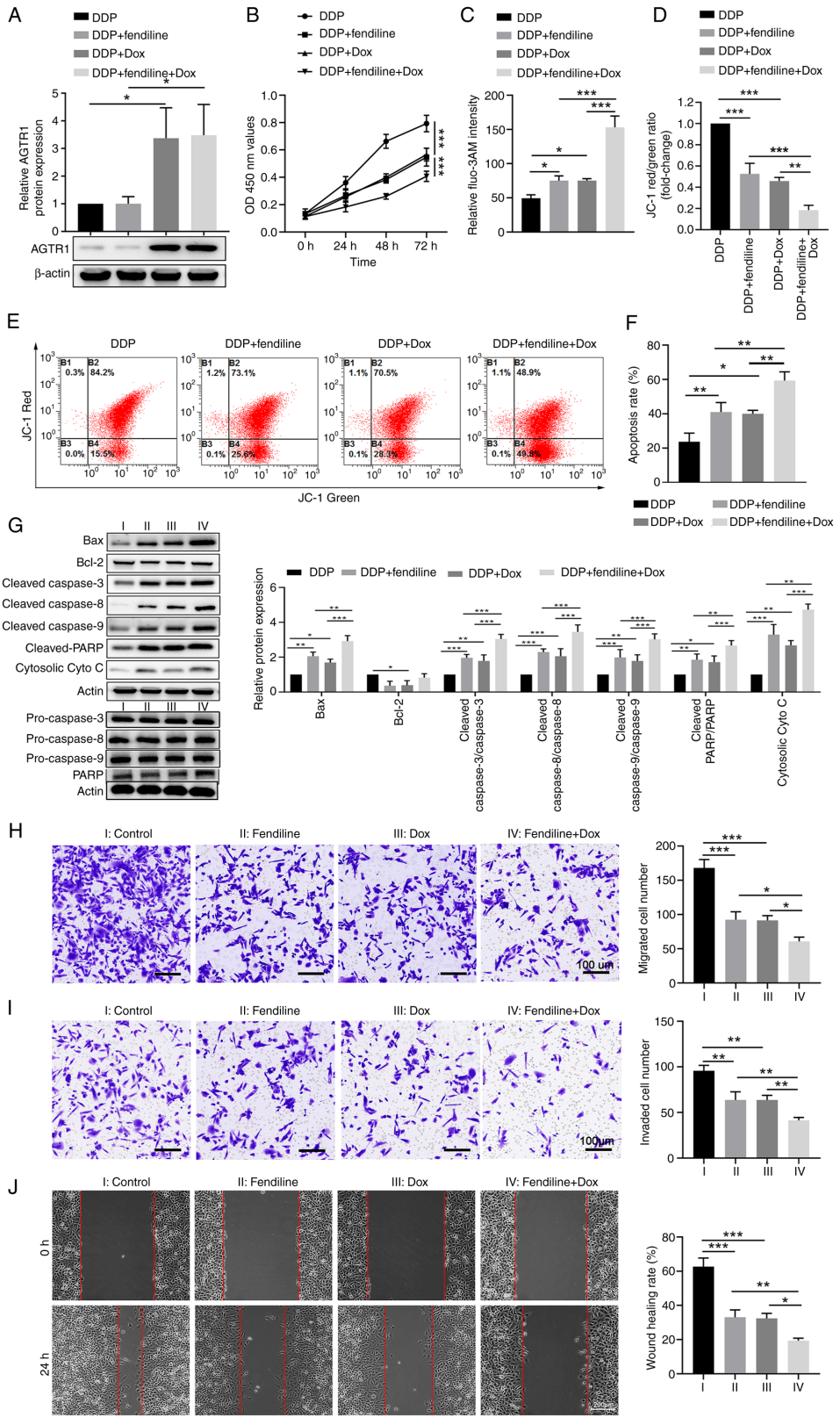

Figure 6. Excessive intracellular Ca^{2+} induced by AGTR1 overexpression and fendiline enhances the chemosensitivity to cisplatin and suppresses the metastasis-relevant traits in esophageal cancer cells. A stable KYSE-150 cell line (pTet-On-AGTR1) with Dox-inducible expression of AGTR1 was generated by transfection of a plasmid bearing the Tet-On system. Cells were treated with cisplatin alone or together with fendiline or Dox, or with both fendiline and Dox for 48 h. (A) The protein expression levels of AGTR1 in the indicated four groups were determined by western blotting. Representative images of the western blot bands are shown and the relative AGTR1 levels were semi-quantified. (B) Cell proliferation and (C) intracellular Ca^{2+} levels in the indicated four groups were determined by Cell Counting Kit-8 assay and flow cytometry analysis of Fluo-3AM staining, respectively. (D) The mitochondrial membrane potentials of cells in the specified four groups were determined by JC-1 staining. (E) Representative flow profiles are shown. Apoptosis of KYSE-150 cells from the indicated four groups was quantitated by (F) flow cytometry and (G) western blotting. The Tet-on KYSE-150 cells were left untreated or treated with fendiline and/or Dox. The (H) migration, (I) invasion and (J) wound healing ability of cells in the indicated four groups were measured. Representative images are shown, and the numbers of migrated/invaded cells and wound healing rates were quantified. n=5 for each group. *P<0.05, **P<0.01, ***P<0.001. Dox, doxycycline; AGTR1, angiotensin II receptor type 1.

with these findings, tumor cells that received both cisplatin and fendiline or both cisplatin and Dox displayed significantly lower cell proliferation and more apoptosis than the cells that received only cisplatin (Figs. 6B and S4B). As expected, the mice that received all the drugs (cisplatin, Dox and fendiline) exhibited the slowest tumor cell proliferation according to Ki67 IHC staining of tumor tissue (Fig. 7D) and the highest level of tumor cell apoptosis (Fig. 7E).

To verify that the enhanced chemo-sensitivity to cisplatin by fendiline and AGTR1 overexpression was associated with increased intracellular Ca^{2+} levels, the expression levels of calcium signaling-associated proteins, including phosphorylated (p-)CAMKK2 (Ser511), p-AMPK (Thr172) and p-mTOR (Ser2448) were examined. As shown in Fig. 7F, a similar trend to that of the apoptosis rate in EC tissues was found. That is, the tumor tissues from mice that received fendiline or Dox had higher levels of the aforementioned calcium signaling-associated proteins than that from mice that received only cisplatin, while tissues from mice that received all the drugs had the highest levels of the calcium signaling-associated proteins. Collectively, these observations in the animal model indicate that it is feasible to use fendiline to increase the sensitivity of EC cells to cisplatin chemotherapy *in vivo*.

Discussion

The incidence of EC shows an alarming increasing trend in Asia and globally, and the mortality rate is still high despite the available systemic treatments (31-33). Since cisplatin-based chemotherapy is one part of the popular treatment regimens for EC (6,34), it is urgent to find new therapeutic targets and develop new treatment approaches to fully potentiate the antitumor efficacy of cisplatin. In the present study, AGTR1 was identified as a potential prognostic marker and therapeutic target. AGTR1 expression was found to enhance the chemo-sensitivity of KYSE-150 and EC109 cells, and markedly decrease their metastasis-relevant traits. Notably, it was found that the tumor-suppressive function of upregulated AGTR1 was associated with upregulated intracellular Ca^{2+} levels and increased mitochondria-dependent apoptosis. These results provide insights into the functional role of the AGTR1 and Ca^{2+} influx in EC treatments and suggest that they are potential targets for amplifying the efficacy of cisplatin-mediated chemotherapy in EC.

AGTR1 is a component of the renin angiotensin system. AGTR1 classically regulates cardiovascular homeostasis and has shown the potential to stimulate cell proliferation, migration or invasion, and promote angiogenesis, inflammation and immunity (19). Increasing evidence shows that the inhibitory effect of losartan and candesartan on AGTR1 can inhibit angiogenesis, which helps to inhibit tumor growth and blood metastasis (35,36). For instance, AGTR1-mediated signaling through CXC chemokine receptor 4/stromal cell derived factor 1α was reported to regulate breast cancer migration and lymph node metastasis (19). It was also found that AGTR1 activation in ovarian cancer significantly enhanced multicellular spheroids formation and increased peritoneal metastasis via upregulation of lipid desaturation and suppression of endoplasmic reticulum stress (37). It is of note that two recent reports also revealed a positive correlation between AGTR1 expression and the proliferation of human EC cells (38,39). Li *et al* (38) found that AGTR1 upregulation in ESCC was univariately associated with inferior overall survival and remained multivariately independent, and angiotensin II stimulated the growth of ESCC cells *in vitro*. Fujihara *et al* (39) reported that the AGTR1 antagonist, telmisartan, suppressed the proliferation and tumor growth of human esophageal adenocarcinoma cells by inducing cell cycle arrest via the AMPK/mTOR pathway. Contrary to the report from Li *et al* (38), an adverse association between ATGR1 expression and the outcome of patients with EC after treatment was identified in the present study. This discrepancy may be due to the differences in geographical location, disease stages and treatment regimens in the selected patient cohorts. In addition, in their study models, either angiotensin II or the AGTR1 antagonist, telmisartan, was employed, while the models in the present study involved merely the manipulation of the AGTR1 expression levels in EC cells, which might more faithfully reflect the relationship between AGTR1 expression and EC disease progression.

Multiple aspects of the molecular mechanisms of the angiotensin II/AGTR1 axis and the use of an AGTR1 antagonist in controlling cancer disease progression were proposed (37), such as upregulation of lipid desaturation and suppression of endoplasmic reticulum stress. The present study focused on whether AGTR1 regulates the intracellular Ca^{2+} level and induces apoptosis in EC cells. After activation by the vasoconstricting peptide, angiotensin II, AGTR1 is coupled with Gq/11 to activate phospholipase C and increase the concentration of cytoplasmic Ca^{2+}, which triggers cellular responses, such as stimulation of protein kinase C, inhibition of adenylate cyclase and activation of various tyrosine kinases (40). The stored Ca^{2+} is released from the endoplasmic reticulum and taken up by mitochondria, triggering cell apoptosis (41,42). The accumulation of Ca^{2+} in mitochondria leads to an increase in mitochondrial membrane permeability by stimulating the opening of the mitochondrial permeability transition pore (mPTP). The opening of the mPTP leads to the release of pro-apoptotic factors, particularly cytochrome C (41,42). The results of the present study showed that the expression levels of AGTR1 in both KYSE-150 cells and EC109 cells were positively associated with their apoptotic rates, intracellular Ca^{2+} levels, mitochondrial membrane potential loss and level of released cytochrome C. These results indicated that AGTR1 overexpression can induce Ca^{2+} influx in EC cells and the mitochondrial calcium overload can trigger apoptotic cell death. Moreover, the reduced migration and invasion abilities of EC cell lines upon AGTR1 overexpression might at least be partially due to AGTR1-mediated apoptotic cell death through the mitochondria-dependent pathway. Consistently, repression of the AGTR1 gene was found to promote the multi-chemoresistance of osteosarcoma, indicating that AGTR1 is a potential target for the effective chemotherapy of osteosarcoma (22). Additionally, in accordance with the previous results showing AGTR1-induced apoptosis in other cell types including intestinal epithelial (25) and cardiac (26) cells, the results of the present study suggest that AGTR1 is a new therapeutic target in EC, and drug screening for activating the function of AGTR1 in triggering Ca^{2+} influx-mediated apoptosis may be useful to develop new drugs to treat EC.

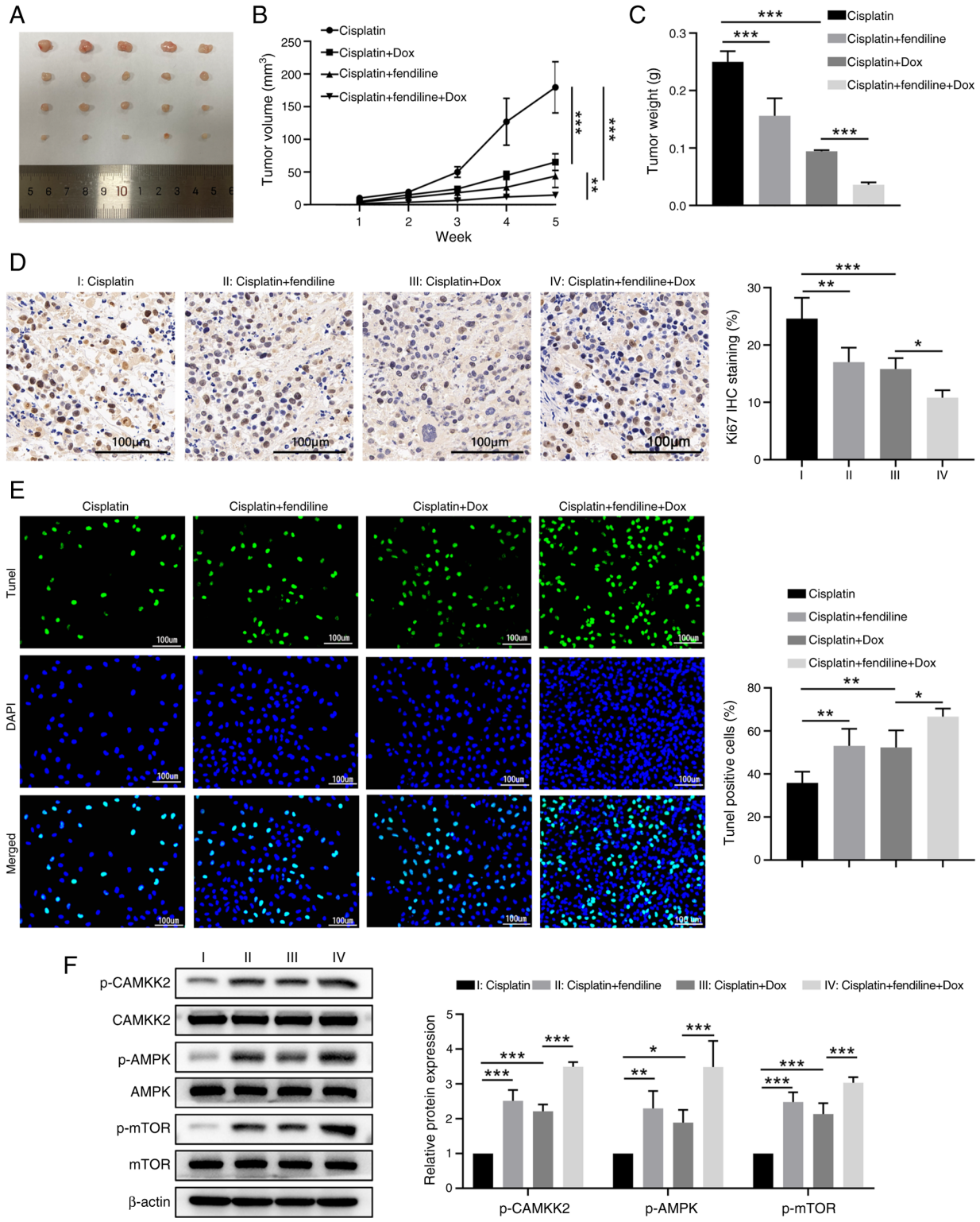

Figure 7. Fendiline administration and induced AGTR1 overexpression sensitizes grafted esophageal cancer cells to cisplatin chemotherapy in a mice model. Nude mice were injected with the Tet-on KYSE-150 cells. At 7 days after tumor growth, nude mice were treated with cisplatin alone, cisplatin + fendiline, cisplatin + Dox or cisplatin + fendiline + Dox. Tumor volume was monitored once per week and tumor tissues were collected at 36 days after tumor inoculation. (A) Tumor image of the indicated four groups. (B) Tumor growth curves of the indicated four groups. (C) Tumor weight at the end time-point. (D) Cell proliferation in tumor tissues was determined by Ki-67 staining. (E) Apoptosis of tumor tissues was determined by TUNEL assay. (F) The levels of calcium signaling-associated proteins in tumor tissues were determined by western blotting. Representative images of the western blot bands are shown and the relative protein levels were semi-quantified. n=5 for each group. *P<0.05, **P<0.01, ***P<0.001. Dox, doxycycline; AGTR1, angiotensin II receptor type 1; IHC, immunohistochemistry; TUNEL, terminal deoxynucleotidyl transferase dUTP nick-end labeling; p-, phosphorylated.

Initially, as an anti-anginal agent for the treatment of coronary heart disease (43,44), fendiline was shown to bind to the Ca^{2+} channel and calmodulin, thus inhibiting the transient outward current in rat ventricular cardiomyocytes (45)

and L-type Ca^{2+} channels in ventricular myocytes from rats and guinea pigs (46,47). In contrast to its inhibition of Ca^{2+} channels, fendiline was found to be able to induce a rise in intracellular Ca^{2+} level in different cells by causing extracellular Ca^{2+} influx and intracellular Ca^{2+} release from the endoplasmic reticulum (48,49). The possibility of utilizing fendiline to evoke Ca^{2+} influx and subsequent cell death in multiple cancer types has been explored. The efficacy of fendiline as anti-malignancy drug, including inhibition of proliferation and invasion as well as the induction of cell death were demonstrated in human oral cancer (50), pancreatic cancer (51), bladder carcinoma (52), hepatoma (53) and human osteosarcoma (54) cells. It is worth noting that fendiline is reported to enhance the cytotoxic effects of other therapeutic agents. For instance, the combinational use of fendiline with inhibitors such as gemcitabine, visudyne, a Yes-associated protein 1 inhibitor or tivantinib (ARQ197, a c-Met inhibitor) can overcome the growth and oncogenic characteristics of pancreatic cancer cells (55). Additionally, co-administration of fendiline hydrochloride was reported to enhance the chemotherapeutic efficacy of cisplatin in neuroblastoma treatment, as evidenced by the enhanced ability of cisplatin to induce the apoptosis of neuroblastoma cells and a reduction in tumor growth and prolonged animal survival rate in a xenograft mice model (56). In line with these findings, the present study found that fendiline treatment increased the cytotoxic potency of cisplatin in KYSE-150 cells both *in vitro* and *in vivo*, suggesting that administration of fendilin may be a potential novel therapeutic method to improve the efficacy of cisplatin in invasive and poorly responsive EC cases.

Of note, in the xenograft mice model established in the present study, increased expression levels of Ca^{2+} signaling-related molecules (including p-AMPK and p-mTOR) in tumor tissues from the cisplatin + fendiline group and the Dox + fendiline group were observed, compared with the cisplatin alone group. This is similar to another study, in which telmisartan inhibited human esophageal adenocarcinoma cell proliferation and growth via the AMPK/mTOR pathway (39). Moreover, as this drug combination showed enhanced efficacy, the dose of cisplatin could be decreased to minimize the adverse effects of cisplatin treatments. Furthermore, it has been reported that fendiline inhibited the proliferation of lung, pancreatic, endometrial and colon tumor cells expressing oncogenic mutant K-Ras more effectively than those of tumor cells expressing wild-type K-Ras, which indicates that fendiline is a selective inhibitor of carcinogenic K-Ras function, regardless of tumor origin (56). Therefore, the implication of the findings of the present study could be extended to treating EC and other types of malignancies with oncogenic mutant K-Ras expression in a more efficient way by combinational administration of fendiline and other therapeutics.

The present study has several limitations. First, the sample size of patients with EC for the quantitation of AGTR1 expression was limited. The patients included in the present study were also drawn from a single institution and thus were subject to referral bias. A study with data from multiple centers with different geographical locations, disease stages and treatment regimens may be necessary to further validate the study findings. Second, the present study did explore the signaling pathway mechanisms involved in AGTR1 and the detailed molecular mechanisms underlying the regulation of EC apoptosis. In the future, predictions through bioinformatics analysis could be made, and the combined *in silico* study and experimental investigation could facilitate the identification of more interacting genes to locate the detailed downstream pathways of AGTR1 in EC. Third, the experiments merely showed the add-on effects of cisplatin, fendiline and induced AGTR1 overexpression in EC cells. More insensitive investigations are needed to clarify whether the co-administration regimens with reduced doses still work efficiently and how a synergistic effect could be achieved to further minimize the therapeutic doses.

In summary, the results of the present study indicated that AGTR1 expression-mediated Ca^{2+} influx suppressed the oncogenic traits of EC cells and increased apoptosis via the mitochondrial pathway, which can be utilized to enhance the chemosensitivity of cisplatin in EC treatment. Notably, increasing the intracellular Ca^{2+} levels by co-administration of fendiline reinforced the cytotoxic efficacy of cisplatin both *in vitro* and *in vivo*. These findings shed new light on the functional role of Ca^{2+} influx-induced cell death in EC and provide a mechanistic insight into using fendiline to potentiate the chemotherapy efficacy of cisplatin in patients with EC.

Acknowledgements

Not applicable.

Funding

This study was supported by the National Natural Science Foundation of China (grant no. 82203851), Nanchong Science and Technology Program (grant nos. 22SXQT0340, 22SXQT0336, 20SXQT0328, 20SXQT0325, 20SXPTJS0003, 20SXQT0074 and 20SXQT0181) and Doctoral Fund of North Sichuan Medical College (grant no. CBY22-QDA01).

Availability of data and materials

The RNA sequencing data generated in the present study may be found in the Gene Expression Omnibus database under accession number GSE263647 or at the following URL: https://www.ncbi.nlm.nih.gov/geo/query/acc.cgi?acc=GSE263647. All other data generated in the present study may be requested from the corresponding author.

Authors' contributions

KL, JB and RZ confirm the authenticity of all the raw data. Conception and design were conducted by KL, JB, RZ, RX and LP; acquisition of data (acquired and managed patients and provided facilities) was conducted by YL, SY and GF; analysis and interpretation of data (such as statistical, biostatistics and computational analyses) was conducted by KL, GS and JB; writing and/or revising the manuscript was conducted by RZ and RX; administrative, technical or material support (such as reporting or organizing data and constructing databases) was conducted by LP and YL; study supervision was conducted by KL. All authors read and approved the final version of the manuscript.

Ethics approval and consent to participate

Written informed consent was obtained from all patients and the study protocol was approved by the Medical Ethics Committee of Nanchong Central Hospital (approval no. 2019.095; Nanchong, China). Animal care and study were approved by the Ethics Committee of North Sichuan Medical College (approval no. NSMC202144; Nanchong, China).

Patient consent for publication

Not applicable.

Competing interests

The authors declare that they have no competing interests.

References

1. Huang FL and Yu SJ: Esophageal cancer: Risk factors, genetic association, and treatment. Asian J Surg 41: 210-215, 2018.
2. Sung H, Ferlay J, Siegel RL, Laversanne M, Soerjomataram I, Jemal A and Bray F: Global cancer statistics 2020: GLOBOCAN estimates of incidence and mortality worldwide for 36 cancers in 185 countries. CA Cancer J Clin 71: 209-249, 2021.
3. Arnal MJ, Arenas AF and Arbeloa AL: Esophageal cancer: Risk factors, screening and endoscopic treatment in Western and Eastern countries. World J Gastroenterol 21: 7933-7943, 2015.
4. Yang YM, Hong P, Xu WW, He QY and Li B: Advances in targeted therapy for esophageal cancer. Signal Transduct Target Ther 5: 229, 2020.
5. Borggreve AS, Kingma BF, Domrachev SA, Koshkin MA, Ruurda JP, van Hillegersberg R, Takeda FR and Goense L: Surgical treatment of esophageal cancer in the era of multimodality management. Ann N Y Acad Sci 1434: 192-209, 2018.
6. Ku GY: Systemic therapy for esophageal cancer: Chemotherapy. Chin Clin Oncol 6: 49, 2017.
7. Luan S, Zeng X, Zhang C, Qiu J, Yang Y, Mao C, Xiao X, Zhou J, Zhang Y and Yuan Y: Advances in drug resistance of esophageal cancer: From the perspective of tumor microenvironment. Front Cell Dev Biol 9: 664816, 2021.
8. Ilson DH, Forastiere A, Arquette M, Costa F, Heelan R, Huang Y and Kelsen DP: A phase II trial of paclitaxel and cisplatin in patients with advanced carcinoma of the esophagus. Cancer J 6: 316-323, 2000.
9. Li Z, Zhang P, Ma Q, Wang D and Zhou T: Cisplatin-based chemoradiotherapy with 5-fluorouracil or pemetrexed in patients with locally advanced, unresectable esophageal squamous cell carcinoma: A retrospective analysis. Mol Clin Oncol 6: 743-747, 2017.
10. Dasari S and Tchounwou PB: Cisplatin in cancer therapy: Molecular mechanisms of action. Eur J Pharmacol 740: 364-378, 2014.
11. Cui C, Merritt R, Fu L and Pan Z: Targeting calcium signaling in cancer therapy. Acta Pharm Sin B 7: 3-17, 2017.
12. Dubois C, Abeele FV and Prevarskaya N: Targeting apoptosis by the remodelling of calcium-transporting proteins in cancerogenesis. FEBS J 280: 5500-5510, 2013.
13. Al-Bahlani S, Fraser M, Wong AY, Sayan BS, Bergeron R, Melino G and Tsang BK: P73 regulates cisplatin-induced apoptosis in ovarian cancer cells via a calcium/calpain-dependent mechanism. Oncogene 30: 4219-4230, 2011.
14. Gualdani R, de Clippele M, Ratbi I, Gailly P and Tajeddine N: Store-Operated calcium entry contributes to cisplatin-induced cell death in non-small cell lung carcinoma. Cancers (Basel) 11: 430, 2019.
15. Shen L, Wen N, Xia M, Zhang YU, Liu W, Xu YE and Sun L: Calcium efflux from the endoplasmic reticulum regulates cisplatin-induced apoptosis in human cervical cancer HeLa cells. Oncol Lett 11: 2411-2419, 2016.
16. Singh KD and Karnik SS: Angiotensin receptors: Structure, function, signaling and clinical applications. J Cell Signal (Los Angel) 1: 111, 2016.
17. Barreras A and Gurk-Turner C: Angiotensin II receptor blockers. Proc (Bayl Univ Med Cent) 16: 123-126, 2003.
18. Rhodes DR, Ateeq B, Cao Q, Tomlins SA, Mehra R, Laxman B, Kalyana-Sundaram S, Lonigro RJ, Helgeson BE, Bhojani MS, *et al*: AGTR1 overexpression defines a subset of breast cancer and confers sensitivity to losartan, an AGTR1 antagonist. Proc Natl Acad Sci USA 106: 10284-10289, 2009.
19. Ma Y, Xia Z, Ye C, Lu C, Zhou S, Pan J, Liu C, Zhang J, Liu T, Hu T, *et al*: AGTR1 promotes lymph node metastasis in breast cancer by upregulating CXCR4/SDF-1alpha and inducing cell migration and invasion. Aging (Albany NY) 11: 3969-3992, 2019.
20. Ateeq B, Tomlins SA and Chinnaiyan AM: AGTR1 as a therapeutic target in ER-positive and ERBB2-negative breast cancer cases. Cell Cycle 8: 3794-3795, 2009.
21. Suganuma T, Ino K, Shibata K, Kajiyama H, Nagasaka T, Mizutani S and Kikkawa F: Functional expression of the angiotensin II type 1 receptor in human ovarian carcinoma cells and its blockade therapy resulting in suppression of tumor invasion, angiogenesis, and peritoneal dissemination. Clin Cancer Res 11: 2686-2694, 2005.
22. Pu Y, Zhao F, Li Y, Cui M, Wang H, Meng X and Cai S: The miR-34a-5p promotes the multi-chemoresistance of osteosarcoma via repression of the AGTR1 gene. BMC Cancer 17: 45, 2017.
23. Kooptiwut S, Hanchang W, Semprasert N, Junking M, Limjindaporn T and Yenchitsomanus PT: Testosterone reduces AGTR1 expression to prevent β-cell and islet apoptosis from glucotoxicity. J Endocrinol 224: 215-224, 2015.
24. Kooptiwut S, Wanchai K, Semprasert N, Srisawat C and Yenchitsomanus PT: Estrogen attenuates AGTR1 expression to reduce pancreatic β-cell death from high glucose. Sci Rep 7: 16639, 2017.
25. Wang W, Sun L, Xiao W and Yang H: Essential role of angiotensin receptors in the modulation of intestinal epithelial cell apoptosis. J Pediatr Gastroenterol Nutr 57: 562-569, 2013.
26. Yang Y, Zhou Y, Cao Z, Tong XZ, Xie HQ, Luo T, Hua XP and Wang HQ: miR-155 functions downstream of angiotensin II receptor subtype 1 and calcineurin to regulate cardiac hypertrophy. Exp Ther Med 12: 1556-1562, 2016.
27. Berry MF: Esophageal cancer: Staging system and guidelines for staging and treatment. J Thorac Dis 6 (Suppl 3): S289-S297, 2014.
28. Boonstra JJ, van der Velden AW, Beerens EC, van Marion R, Morita-Fujimura Y, Matsui Y, Nishihira T, Tselepis C, Hainaut P, Lowe AW, *et al*: Mistaken identity of widely used esophageal adenocarcinoma cell line TE-7. Cancer Res 67: 7996-8001, 2007.
29. Capes-Davis A, Theodosopoulos G, Atkin I, Drexler HG, Kohara A, MacLeod RA, Masters JR, Nakamura Y, Reid YA, Reddel RR and Freshney RI: Check your cultures! A list of cross-contaminated or misidentified cell lines. Int J Cancer 127: 1-8, 2010.
30. Livak KJ and Schmittgen TD: Analysis of relative gene expression data using real-time quantitative PCR and the 2(-Delta Delta C(T)) method. Methods 25: 402-408, 2001
31. Liu CQ, Ma YL, Qin Q, Wang PH, Luo Y, Xu PF and Cui Y: Epidemiology of esophageal cancer in 2020 and projections to 2030 and 2040. Thorac Cancer 14: 3-11, 2023.
32. Zhu H, Wang Z, Deng B, Mo M, Wang H, Chen K, Wu H, Ye T, Wang B, Ai D, *et al*: Epidemiological landscape of esophageal cancer in Asia: Results from GLOBOCAN 2020. Thorac Cancer 14: 992-1003, 2023.
33. Uhlenhopp DJ, Then EO, Sunkara T and Gaduputi V: Epidemiology of esophageal cancer: Update in global trends, etiology and risk factors. Clin J Gastroenterol 13: 1010-1021, 2020.
34. Brown A, Kumar S and Tchounwou PB: Cisplatin-Based chemotherapy of human cancers. J Cancer Sci Ther 11: 97, 2019.
35. Chauhan VP, Martin JD, Liu H, Lacorre DA, Jain SR, Kozin SV, Stylianopoulos T, Mousa AS, Han X, Adstamongkonkul P, *et al*: Angiotensin inhibition enhances drug delivery and potentiates chemotherapy by decompressing tumour blood vessels. Nat Commun 4: 2516, 2013.
36. Diop-Frimpong B, Chauhan VP, Krane S, Boucher Y and Jain RK: Losartan inhibits collagen I synthesis and improves the distribution and efficacy of nanotherapeutics in tumors. Proc Natl Acad Sci USA 108: 2909-2914, 2011.
37. Zhang Q, Yu S, Lam MMT, Poon TCW, Sun L, Jiao Y, Wong AST and Lee LT: Angiotensin II promotes ovarian cancer spheroid formation and metastasis by upregulation of lipid desaturation and suppression of endoplasmic reticulum stress. J Exp Clin Cancer Res 38: 116, 2019.

38. Li SH, Lu HI, Chang AY, Huang WT, Lin WC, Lee CC, Tien WY, Lan YC, Tsai HT and Chen CH: Angiotensin II type I receptor (AT1R) is an independent prognosticator of esophageal squamous cell carcinoma and promotes cells proliferation via mTOR activation. Oncotarget 7: 67150-67165, 2016.
39. Fujihara S, Morishita A, Ogawa K, Tadokoro T, Chiyo T, Kato K, Kobara H, Mori H, Iwama H and Masaki T: The angiotensin II type 1 receptor antagonist telmisartan inhibits cell proliferation and tumor growth of esophageal adenocarcinoma via the AMPKalpha/mTOR pathway in vitro and in vivo. Oncotarget 8: 8536-8549, 2017.
40. Guo DF, Sun YL, Hamet P and Inagami T: The angiotensin II type 1 receptor and receptor-associated proteins. Cell Res 11: 165-180, 2001.
41. Rizzuto R, Pinton P, Ferrari D, Chami M, Szabadkai G, Magalhães PJ, Di Virgilio F and Pozzan T: Calcium and apoptosis: Facts and hypotheses. Oncogene 22: 8619-8627, 2003.
42. Giorgi C, Baldassari F, Bononi A, Bonora M, De Marchi E, Marchi S, Missiroli S, Patergnani S, Rimessi A, Suski JM, *et al*: Mitochondrial Ca(2+) and apoptosis. Cell Calcium 52: 36-43, 2012.
43. Schulz J, Lubnau E, Grossmann M and Rück W: Double-blind, randomized study of the anti-anginal and anti-ischaemic efficacy of fendiline and diltiazem in patients with coronary heart disease. Curr Med Res Opin 12: 521-539, 1991.
44. Bayer R and Mannhold R: Fendiline: A review of its basic pharmacological and clinical properties. Pharmatherapeutica 5: 103-136, 1987.
45. Fassbender V, Wegener JW, Shainberg A and Nawrath H: Inhibition by fendiline of the transient outward current in rat ventricular cardiomyocytes. J Cardiovasc Pharmacol 33: 905-911, 1999.
46. Nawrath H, Klein G, Rupp J, Wegener JW and Shainberg A: Open state block by fendiline of L-type Ca++ channels in ventricular myocytes from rat heart. J Pharmacol Exp Ther 285: 546-552, 1998.
47. Tripathi O, Schreibmayer W and Tritthart HA: Fendiline inhibits L-type calcium channels in guinea-pig ventricular myocytes: A whole-cell patch-clamp study. Br J Pharmacol 108: 865-869, 1993.
48. Lin MC and Jan CR: The anti-anginal drug fendiline elevates cytosolic Ca(2+) in rabbit corneal epithelial cells. Life Sci 71: 1071-1079, 2002.
49. Jan CR, Lee KC, Chou KJ, Cheng JS, Wang JL, Lo YK, Chang HT, Tang KY, Yu CC and Huang JK: Fendiline, an anti-anginal drug, increases intracellular Ca2+ in PC3 human prostate cancer cells. Cancer Chemother Pharmacol 48: 37-41, 2001.
50. Huang C, Huang C, Cheng J, Liu S, Chen I, Tsai J, Chou C, Tseng P and Jan C: Fendiline-evoked [Ca2+]i rises and non-Ca2+-triggered cell death in human oral cancer cells. Hum Exp Toxicol 28: 41-48, 2009.
51. Woods N, Trevino J, Coppola D, Chellappan S, Yang S and Padmanabhan J: Fendiline inhibits proliferation and invasion of pancreatic cancer cells by interfering with ADAM10 activation and β-catenin signaling. Oncotarget 6: 35931-35948, 2015.
52. Cheng JS, Wang JL, Lo YK, Chou KJ, Lee KC, Liu CP, Chang HT and Jan CR: Effects of the antianginal drug fendiline on Ca2+ movement in hepatoma cells. Hum Exp Toxicol 20: 359-364, 2001.
53. Wang J, Cheng J, Chan R, Tseng L, Chou K, Tang K, Lee KC, Lo Y, Wang J and Jan C: The anti-anginal drug fendiline increases intracellular Ca(2+) levels in MG63 human osteosarcoma cells. Toxicol Lett 119: 227-233, 2001.
54. Alhothali M, Mathew M, Iyer G, Lawrence HR, Yang S, Chellappan S and Padmanabhan J: Fendiline enhances the cytotoxic effects of therapeutic agents on PDAC cells by inhibiting tumor-promoting signaling events: A potential strategy to combat PDAC. Int J Mol Sci 20: 2423, 2019.
55. Brizzolara A, Garbati P, Vella S, Calderoni M, Quattrone A, Tonini GP, Capasso M, Longo L, Barbieri R, Florio T and Pagano A: Co-Administration of fendiline hydrochloride enhances chemotherapeutic efficacy of cisplatin in neuroblastoma treatment. Molecules 25: 5234, 2020.
56. van der Hoeven D, Cho KJ, Ma X, Chigurupati S, Parton RG and Hancock JF: Fendiline inhibits K-Ras plasma membrane localization and blocks K-Ras signal transmission. Mol Cell Biol 33: 237-251, 2013.